Determination of the Volume Changes Occurring for Conversion/Alloying-Type Li-Ion Anodes upon Lithiation/Delithiation

Jakob Asenbauer, Matthias Kuenzel, Tobias Eisenmann, Adele Birrozzi, Jeng-Kuei Chang, Stefano Passerini, and Dominic Bresser*

ABSTRACT: High-capacity lithium-ion anodes such as alloying-, conversion-, and conversion/alloying-type materials are subjected to extensive volume variation upon lithiation/delithiation. However, a careful examination of these processes at the particle and electrode level as well as the impact of the kind of lithium-ion uptake mechanism is still missing. Herein, we investigated the volume variation upon lithiation/delithiation for a series of conversion/alloying materials with a varying relative contribution of the alloying and conversion reaction, i.e., carbon-coated $ZnFe_2O_4$, $Zn_{0.9}Fe_{0.1}O$, and $Sn_{0.9}Fe_{0.1}O_2$ by *operando* dilatometry and *ex situ* scanning electron microscopy of the electrode cross section. While the theoretical estimation at the particle level indicates a rather large volume expansion of 113% ($ZnFe_2O_4$) and more, the true volume variation on the electrode level reveals very limited changes of only around 11% ($ZnFe_2O_4$). Combining the experimental findings with some theoretical considerations highlights the (to a certain extent unexpected) impact of the initial electrode porosity.

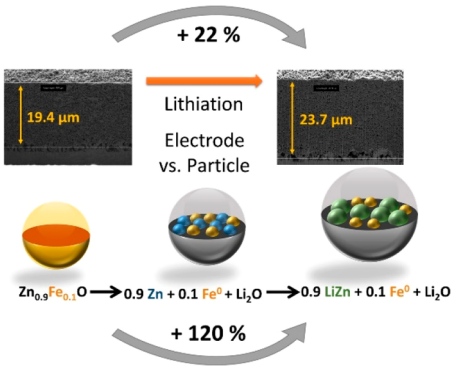

Lithium-ion batteries (LIBs) have attracted great interest in academia and industry as high-performance energy storage devices for portable electronics, (hybrid) electric vehicles, and stationary storage.[1−3] The great majority of commercial LIBs comprise graphite as the active material for the negative electrode, which possesses a very low lithiation/delithiation potential of ca. 0.1 V vs Li^+/Li and a theoretical specific capacity of 372 mAh g^{-1}, thus enabling relatively high energy densities at the full-cell level. However, this low lithiation potential in combination with the rather sluggish Li^+ intercalation kinetics prevents fast charging of the battery cell,[4−6] which is considered now equally as important as high energy densities.[7] Potential alternatives are conversion-type[8−10] or alloying-type active materials.[11,12] These alternative candidates commonly provide substantially higher specific capacities and, frequently, greater rate capability than graphite.[13−15] Nonetheless, both classes of active materials also reveal some fundamental challenges, i.e., a pronounced voltage hysteresis and a rather wide potential window for the complete lithiation/delithiation reaction in the case of conversion-type materials and an extreme volume variation upon lithiation/delithiation in the case of alloying-type compounds.[12,16] To overcome these challenges, the synergistic combination of the two reaction mechanisms in one single material has been proposed.[17] Indeed, such conversion/alloying materials (CAMs) provide elevated specific capacities, high energy densities, stabilized long-term cycling, and excellent rate capability.[18−23] Very recently, we could also show that full cells incorporating CAMs as an anode may provide substantially enhanced energy efficiencies of up to more than 80% and even more than 90% under certain conditions.[21,24,25]

An issue that remains to be investigated, though, is the volume variation upon lithiation/delithiation, which is generally an issue for both conversion-type and alloying-type compounds, resulting in crack formation, loss of electronic contact, particle pulverization, and as a consequence of the latter continuous electrolyte decomposition.[26,27] While these issues can be addressed to a certain extent by nanosizing the active material particles and the application of "buffering" coatings or secondary matrices,[28−30] the negative effect for the battery lifetime remains if the thickness of the electrode keeps changing significantly upon discharge/charge. Accordingly, the initial electrode porosity is considered to play a decisive role.[31,32] The existing (still very limited) literature, however, reports conflicting experimental findings. While Du et al.[33] observed that the porosity in Si-alloy/graphite anodes did not change significantly during cycling, Pietsch et al.[34] reported a decreasing porosity during the lithiation of silicon/graphite negative electrodes. Contrarily, Karkar et al.[35] observed an increasing porosity during the first discharge of silicon/carbon-

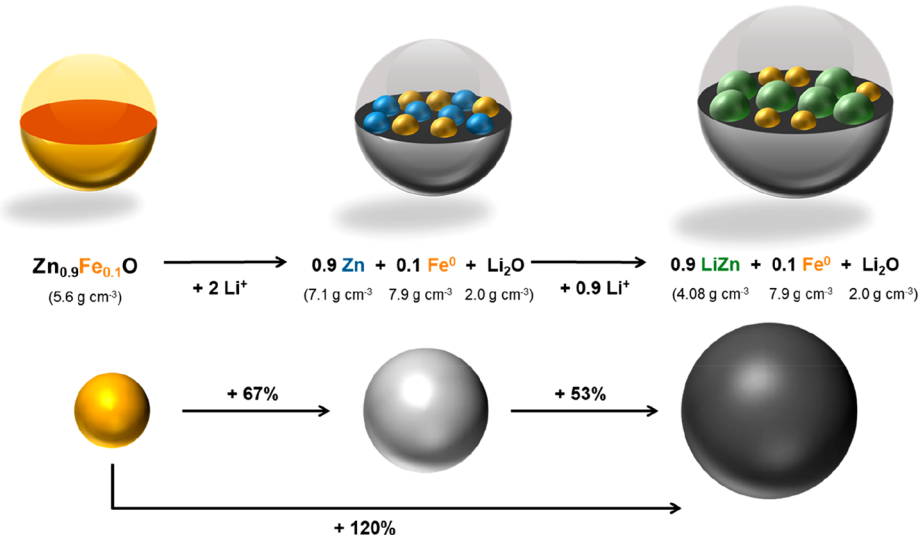

Figure 1. Schematic illustration of theoretical volume changes occurring for $Zn_{0.9}Fe_{0.1}O$ upon lithiation as a result of the initial conversion and subsequent alloying reaction.

based electrodes and generally pointed out that the electrode processing (incl. the calendaring and maturing) as well as the particle/binder interaction play a decisive role. This was further confirmed by Vanpeene et al.[36] who showed that the application of a suitable maturing procedure allows for reduced volume variations and cracking of Si-based electrodes, originating from the possibility of particle sliding and their displacement in the pores during lithiation. Besides these still contradictory findings, comparable studies on conversion-type or conversion/alloying-type active materials are completely missing so far.

Herein, we attempt to fill this gap by investigating the volume variation of CAMs characterized by varying relative contribution of the conversion and alloying reactions, specifically, carbon-coated $ZnFe_2O_4$, $Zn_{0.9}Fe_{0.1}O$, and $Sn_{0.9}Fe_{0.1}O_2$. The investigation is performed by initially comparing the results obtained by *operando* dilatometry and the theoretically expected volume changes. In a subsequent step, we conduct an exemplary *ex situ* cross-sectional scanning electron microscopy analysis of pristine, lithiated, and delithiated $Zn_{0.9}Fe_{0.1}O$–C electrodes and analyze the experimentally observed and theoretically expected volume variation, considering either the total pore volume or the relative porosity constant.

Initially, we estimated the theoretical volume changes of (carbon-coated) $ZnFe_2O_4$, $Zn_{0.9}Fe_{0.1}O$, and $Sn_{0.9}Fe_{0.1}O_2$ based on the density of the nonlithiated and lithiated materials. While the bulk density of the nonlithiated compounds can be determined experimentally, the overall density of the lithiated materials ($\rho_{\text{lithiated}}$) was calculated on the basis of the bulk densities of the different lithiation products (using literature values) according to the formula

$$\rho_{\text{lithiated}} = \frac{1}{\sum_j \frac{\omega_j}{\rho_j}} \tag{1}$$

with ρ_j being the density of each individual phase after lithiation and ω_j its relative mass fraction. A summary of all density values is provided in Table S1, including also the carbon-coated samples having carbon contents of 10 wt % ($ZnFe_2O_4$–C, and $Zn_{0.9}Fe_{0.1}O$–C) and 12 wt % ($Sn_{0.9}Fe_{0.1}O_2$–C). In the following, we describe the (initial) lithiation reaction for these three materials along with the (theoretical) gravimetric capacity values, highlighting the contribution of the conversion and the alloying reaction as well as the corresponding volume changes. The accordingly calculated volumetric capacities are provided in Table S2.

The lithiation of $ZnFe_2O_4$ occurs via the following reactions:[37,38]

$$ZnFe_2O_4 + 8Li^+ + 8e^- \rightarrow 2Fe^0 + 4Li_2O + Zn^0 \tag{2}$$

$$Zn^0 + Li^+ + e^- \rightarrow LiZn \tag{3}$$

The relative contribution of the alloying reaction (3) accounts for 11% in this case, while the total theoretical specific capacity is around 1000 mAh g^{-1}. The estimated volume variation is, thus, largely dominated by the conversion reaction (2), resulting in about 93% volume increase versus a total change of 113% (2 + 3).

For $Zn_{0.9}Fe_{0.1}O$, the relative contribution of the alloying reaction is increased to about 31%, with the overall lithiation taking place via the following reaction mechanism:[23,39,40]

$$Zn_{0.9}Fe_{0.1}O + 2Li^+ + 2e^- \rightarrow 0.1Fe^0 + Li_2O + 0.9Zn^0 \tag{4}$$

$$0.9Zn^0 + 0.9Li^+ + 0.9e^- \rightarrow 0.9LiZn \tag{5}$$

This reaction yields a theoretical specific capacity of 966 mAh g^{-1}. It should be noted that the reaction mechanism is a little more complex with the two mechanisms partially overlapping and employing also the partial alloying of zinc and iron.[40] Nevertheless, we will use herein the simplified mechanism, since the precisely formed (intermediate) species and their ratio are hard to determine quantitatively, while the impact of any overlap of the two reactions is considered to have a negligible impact on the overall volume variation—at least for the given estimation.

As expected, the increase of the relative contribution of the alloying reaction results also in an increased contribution to the theoretical volume change. The volume increase after the conversion reaction (4) is calculated to be 67%, while it is

120% after the subsequent alloying reaction (5), i.e., in the fully lithiated state; see also Figure 1 for a schematic illustration of the stepwise volume changes. Comparing these values with those obtained for $ZnFe_2O_4$ reveals that the alloying reaction is characterized by a relatively larger volume variation than the conversion reaction.

To further highlight this, we conducted the same analysis also for $Sn_{0.9}Fe_{0.1}O_2$, which follows the general reaction mechanism given below, with a relative contribution of the alloying reaction (7) of around 50% to the total theoretical capacity of 1477 mAh g^{-1}.

$$Sn_{0.9}Fe_{0.1}O_2 + 4Li^+ + 4e^- \rightarrow 0.1Fe^0 + 2Li_2O + 0.9Sn^0 \quad (6)$$

$$0.9Sn + 3.96Li^+ + 3.96e^- \rightarrow 0.9Li_{4.4}Sn \quad (7)$$

The calculated volume increase is 116% after the conversion reaction (6), rising to 296% after the alloying reaction (7).

Please note that all these reactions refer to the initial lithiation reaction. For the subsequent delithiation reaction, the general processes are essentially reversed, while the eventually formed metal oxide phases have a (quasi-)amorphous structure.[20,40,41] Besides, all the given values have to be taken with care when evaluating any potential practical application, mainly for two reasons. First, it was shown that CAMs commonly benefit from a carbonaceous coating (or alternatively secondary electron-conductive phases[42]) for stable long-term cycling.[19−21,23] Considering the corresponding weight fraction of 10% used herein, its relatively low density compared to metal oxides (see Table S1 for the experimentally determined densities of $ZnFe_2O_4$−C, $Zn_{0.9}Fe_{0.1}O$−C, and $Sn_{0.9}Fe_{0.1}O_2$−C), and assuming a negligible volume (and density) variation for the carbon coating upon lithiation, the overall volume expansion decreases to "only" 77%, 91%, and 175% for $ZnFe_2O_4$−C, $Zn_{0.9}Fe_{0.1}O$−C, and $Sn_{0.9}Fe_{0.1}O_2$−C, respectively. The second important aspect to be considered is that common electrodes contain also conductive additives and a polymer binder, accompanied by significant porosity. Beattie et al.[43] showed that the electrode expansion correlates with the volume fraction of the active material and that additional, electrochemically inactive phases (such as conductive carbon) have a diluting effect. Thus, we kept the composition of all electrodes studied herein constant to ensure comparability.

To investigate the volume variation at the electrode level, *operando* electrochemical dilatometry was performed for electrodes based on $ZnFe_2O_4$−C, $Zn_{0.9}Fe_{0.1}O$−C, and $Sn_{0.9}Fe_{0.1}O_2$−C. We may note here that this technique determines changes in thickness, i.e., only in one dimension, while any volume change apparently might occur in three dimensions. Nonetheless, given the lateral confinement of the electrode, we may consider the changes in the vertical direction (i.e., in thickness) roughly equivalent to the total volume changes. The results for two and half consecutive cycles are presented in Figure 2 and all results are summarized in Table 1. All pristine electrodes had an initial thickness of l_0 = 18 μm. The volume changes within the first cycle are generally referred to as $l_{lit\ 1}$ for the ("positive") volume change after the first lithiation and as $l_{deli\ 1}$ for the ("negative") volume change after the first delithiation. Accordingly, $l_{deli\ n}$ (with n for the nth cycle) is equivalent to the reversible volume variation $\Delta l_{rev\ n}$, while the difference $\Delta l_{irr\ n} = l_{lit\ n} - l_{deli\ n}$ describes the irreversible expansion during the nth cycle.

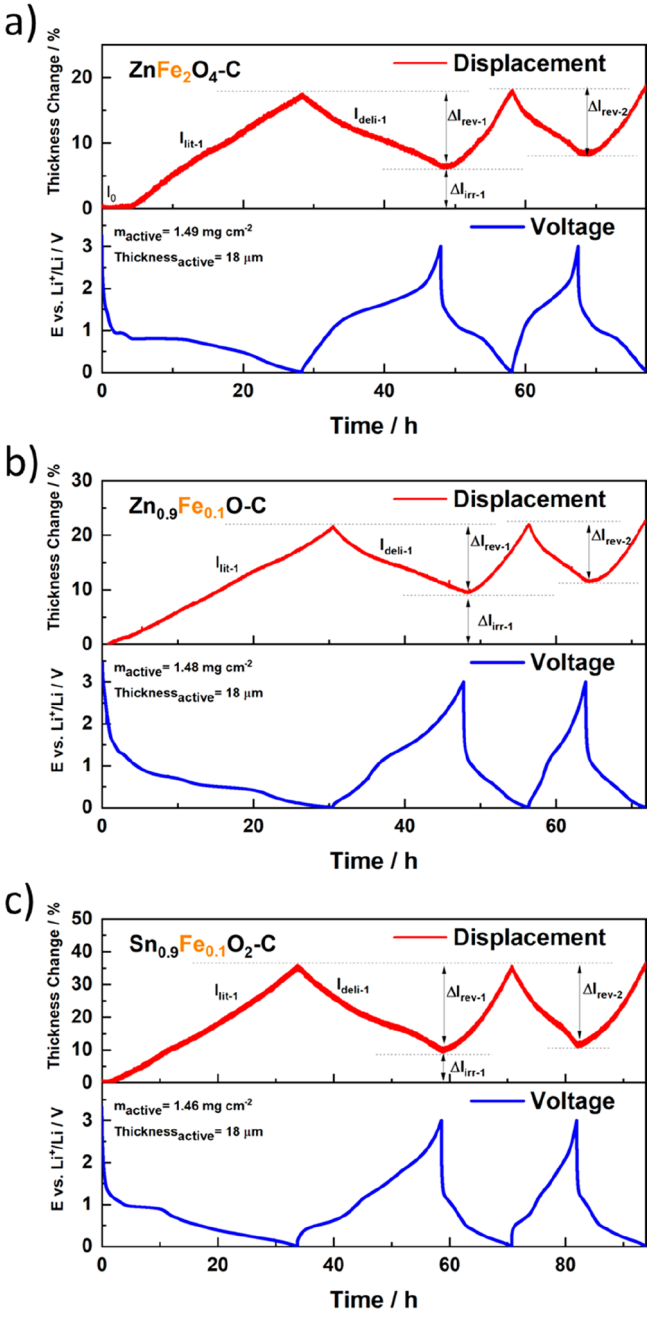

Figure 2. *Operando* dilatometry performed for half-cells comprising working electrodes based on (a) $ZnFe_2O_4$−C, (b) $Zn_{0.9}Fe_{0.1}O$−C, and (c) $Sn_{0.9}Fe_{0.1}O_2$−C as active material. The discharge/charge voltage profiles are given in blue and the corresponding displacement is given in red for each panel (cutoff voltages, 0.01 and 3.0 V vs Li^+/Li; specific current, 50 mA g^{-1} for the first cycle and 100 mA g^{-1} for the second cycle).

Table 1. Summary of Findings for the Reversible and Irreversible Thickness Variations during the First Two Cycles Obtained by *Operando* Dilatometry

active material	l_0/μm	$l_{lit\text{-}1}$/%	$\Delta l_{rev\text{-}1}$/%	$\Delta l_{irr\text{-}1}$/%	$\Delta l_{rev\text{-}2}$/%
$ZnFe_2O_4$−C	18	17.2	10.7	6.5	9.3
$Zn_{0.9}Fe_{0.1}O$−C	18	21.3	11.8	9.5	10.0
$Sn_{0.9}Fe_{0.1}O_2$−C	18	35.0	25.1	9.9	23.2

For $ZnFe_2O_4$−C with the lowest contribution of the alloying reaction (Figure 2a), the initial (short) potential plateau observed has been assigned to the Li^+ insertion into the spinel structure.[23,44] During this plateau, the electrode thickness remains essentially constant, which supports the previous findings,[23,44] as such, a reaction is not considered to result in appreciable volume changes, especially given the rather low degree of lithium uptake. Subsequently, a steady increase in thickness is observed, which amounts to $l_{lit\ 1}(ZnFe_2O_4{-}C)$ = 17.2% at the end of the first lithiation. Upon delithiation the thickness decreases by 10.7% ($\Delta l_{rev\ 1}$), which results in an irreversible expansion of $\Delta l_{irr\ 1}$ = 6.5%. This irreversible fraction presumably originates from the formation of the solid electrolyte interphase and structural rearrangements within the electrode.[45,46] In addition, the formation of (quasi-)amorphous phases upon the first lithiation and the preservation of such (quasi-)amorphous structure during the subsequent delithiation (instead of a reformation of the initial crystalline phase) certainly adds to such initial irreversibility, since amorphous materials are commonly characterized by lower bulk densities.[47] Meanwhile, in the second cycle, the reversible thickness variation decreases to around 9.3% ($\Delta l_{rev\ 2}$). In line with the earlier calculation, the change in thickness is more pronounced for the de/alloying reaction at low potentials (below ∼0.7 V) compared to the conversion reaction.

For $Zn_{0.9}Fe_{0.1}O$−C (Figure 2b), the general evolution is very similar. The electrode coating layer thickness increases initially by $l_{lit\ 1}(Zn_{0.9}Fe_{0.1}O{-}C)$ = 21.3% and decreases subsequently by 11.8% ($\Delta l_{rev\ 1}$), resulting in an irreversible thickness change $\Delta l_{irr\ 1}$ of 9.5%. These values are slightly higher compared to $ZnFe_2O_4$, which is assigned to the relatively higher contribution of the alloying reaction (ca. 31%) and the larger structural rearrangement occurring upon lithiation. In fact, also the reversible thickness variation in the second cycle upon lithiation/delithiation ($\Delta l_{rev\ 2}$ = 10%) is slightly higher compared to $ZnFe_2O_4$−C. Nonetheless, it is lower than for the first cycle, indicating that the volume changes occurring at the electrode level during the subsequent cycles are somehow stabilizing.

The general trend of an increasing variation in thickness with an increasing contribution of the alloying reaction is further confirmed by the *operando* dilatometry results obtained for $Sn_{0.9}Fe_{0.1}O_2$−C, which also owns the highest density in the delithiated state (Table S1). Indeed, the initial increase in thickness, $l_{lit\ 1}$, was found to be 35.0%, with an irreversible fraction of $\Delta l_{irr\ 1}$ = 9.9% and a reversible expansion of $\Delta l_{rev\ 1}$ = 25.1%. For the second cycle, the reversible thickness variation accounts for 23.2%. We may note here that the given irreversible/reversible thickness variation occurs in a rather wide voltage range from 0.01 to 3.0 V. This has been shown to be detrimental for the energy efficiency and energy density at the full-cell level as well as for the continuous SEI (re)formation[20,24,25,40] and, especially in the case of transition metal doped SnO_2, also for the cycling stability.[20,24,40,48] Accordingly, and with respect to the shape of the displacement curve, it is reasonable to say that the thickness variation in a full-cell, when cycling the anode with a limited capacity and, thus, in a narrower voltage range, will be substantially less and ideally only a few percent (depending on the final limitation in voltage and anode capacity utilization). In fact, commercial graphite-based lithium-ion cells also show some variation in thickness, the extent of which depends on the kind of graphite and the overall cell design (including the current collector, separator, packaging, etc.).[49] For instance, an initial irreversible increase in thickness of around 2% ($\Delta l_{irr\ 1}$) has been reported for commercial lithium-ion cells, accompanied by a reversible thickness change of about 2−4% ($\Delta l_{rev\ n>1}$),[49] highlighting that a certain reversible volume variation appears acceptable for commercial cells. Nonetheless, the pronounced increase in thickness upon the first lithiation underlines the importance of optimized electrode architectures and the development of suitable prelithiation strategies.[50,51]

To further discuss the volume variation observed at the electrode level, the electrode porosity as an important parameter has to be taken into account.[31,52] To investigate this experimentally, we performed a representative *ex situ* SEM analysis of the FIB-derived cross section of $Zn_{0.9}Fe_{0.1}O$−C electrodes. EDX mapping of the cross section of the pristine electrode (Figure 3a) reveals that the coating layer thickness is

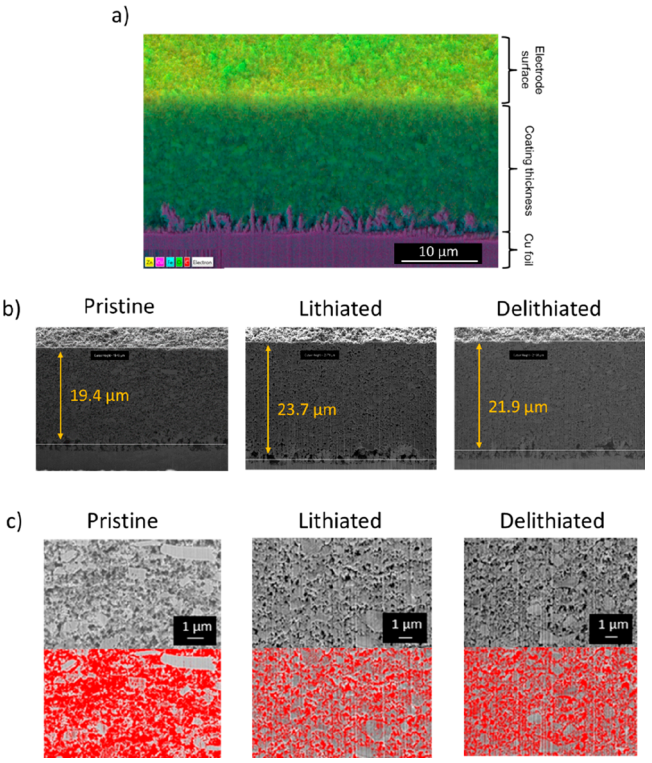

Figure 3. (a) EDX mapping of the FIB-derived cross section of an electrode based on $Zn_{0.9}Fe_{0.1}O$−C as the active material. Zn is colored in yellow, Cu in purple, Fe in light blue, O in light green, and C in red. (b) Comparison of the thickness of the electrode coating layer in the pristine (left), lithiated (middle), and delithiated (right) state. (c) Magnification of the cross sections shown in (b) and determination of the porosity (in red) via computational segmentation.

rather homogeneous and that the active material and the conductive carbon are well distributed within the coating, while there is a significant porosity that might potentially serve as a buffer for the volume changes occurring. Upon lithiation and delithiation, the thickness of the coating layer increases from 19.4 to 23.7 μm and subsequently decreases to 21.9 μm (Figure 3b). These changes translate into a thickness increase upon lithiation of 22.1% and an irreversible (remaining) increase of about 12.8% (i.e., a reversible thickness variation of 9.3%), which is in very good agreement with the findings obtained by *operando* dilatometry (Figure 2 and Table 1). The minor deviation might be explained by some side reactions of

the highly reactive lithiated electrode with, e.g., traces of oxygen in the glovebox, even though the oxygen content was kept well below 0.1 ppm throughout the experiment. In order to determine the impact of the electrode porosity, we had a closer look at the electrode cross section (Figure 3c and Figure S1). Generally, it is observed that the porosity is substantially reduced after the lithiation step and that it remains lower than for the pristine electrode, also after the subsequent delithiation. To quantify these changes in porosity, we used the software ImageJ. It should be noted here that it is not feasible to accurately measure the 3D porous structure on the basis of a 2D image and that instrumental restrictions limit resolving very small pore features. As a consequence, the porosity is commonly underestimated.[53] Nonetheless, for the direct comparison of the porosity in the pristine, lithiated, and delithiated state, this methodology appears suitable. Accordingly, the porosity of the pristine electrode was determined to be 55%. It decreases to 33% in the lithiated state and slightly increases again to 37% after delithiation. This finding indicates that the SEI formation at the active material particle surface and, potentially, some rearrangement of the electrode architecture, are dominating the variation in porosity, while the (reversible) volume changes of the $Zn_{0.9}Fe_{0.1}O$ particles have a relatively minor impact.

To better understand the impact of the electrode porosity, we conducted some fundamental calculations. The porosity P of a composite electrode A (i.e., P_A) is defined as the ratio of the void volume V_V of the total volume V_T. It can be calculated with the density of the electrode coating layer ρ_A and the theoretical density of the composite ρ_T according to

$$P_A = \frac{V_V}{V_T} = 1 - \frac{\rho_A}{\rho_T} \tag{8}$$

While ρ_A can be easily derived by measuring the diameter, the thickness, and the mass of the electrode film, ρ_T can be calculated according to

$$\rho_T = \frac{1}{\sum_i \frac{\omega_i}{\rho_i}} \tag{9}$$

with ω_i being the weight fraction of any component i of the composite electrode and ρ_i being its density. Accordingly, eq 8 can be written as

$$P_A = \frac{V_V}{V_T} = 1 - \frac{\rho_A}{\rho_T} = 1 - \rho_A \sum_i \frac{\omega_i}{\rho_i} \tag{10}$$

The measured densities of the active materials are summarized in Table S1 and the densities of the conductive carbon (Super C65) and the CMC binders were measured to be 1.8 and 1.6 g cm^{-3}, respectively. According to eq 10, the herein studied electrodes, based on $ZnFe_2O_4$−C, $Zn_{0.9}Fe_{0.1}O$−C, and $Sn_{0.9}Fe_{0.1}O_2$−C as active materials, have similar calculated porosity values of 65%, 66%, and 67%, respectively. These values are somewhat higher than the experimentally determined value of 55% (examined using ImageJ) in the case of $Zn_{0.9}Fe_{0.1}O$−C, which is ascribed to the earlier mentioned underestimation in the latter case. In addition, it might be that the density of, e.g., the polymer is different in such a composite electrode compared to its "bulk" state due to the interaction with the active material particles and the conductive carbon. Hence, the eventual "real" density of the coating layer and, thus, the porosity might differ slightly from the calculated value.

In a next step, we defined different scenarios for the evolution of the electrode porosity upon lithiation/delithiation. Since there are still pores observed also for the lithiated electrode (Figure 3c) and as there has been a significant increase in thickness recorded by both *operando* dilatometry (Figure 2) and *ex situ* SEM/FIB analysis (Figure 3), while the latter revealed that the changes in porosity are largely dominated by SEI formation and other irreversible processes, it is apparent that the given porosity does not completely "absorb" the volume expansion occurring. We may briefly note that the following considerations focus, indeed, solely on the volume changes at the electrode level induced by the (theoretical) reversible volume variation at the particle level.

First, we assumed that the overall porosity would remain constant upon lithiation/delithiation. In such a case, the pores would expand to the same extent as the volume of the active material during lithiation and the availability of void space in the electrode would not buffer the volume expansion at all. Following these considerations, the volume would increase by 41%, 46%, and 90% for $ZnFe_2O_4$−C, $Zn_{0.9}Fe_{0.1}O$−C, and $Sn_{0.9}Fe_{0.1}O_2$−C, respectively (see also Figure 4a). Obviously, these values largely exceed the values experimentally determined for the reversible volume changes. Hence, despite the *ex situ* SEM results, the initial porosity plays a role for the relatively limited reversible volume variation at the electrode level.

Second, we assumed a constant pore volume, meaning that the relative porosity at a given volume decreases with the total increase in volume of the electrode as a whole upon lithiation. In this case, the volume of the electrode would increase by 13.6%, 14.7%, and 28.6% for $ZnFe_2O_4$−C, $Zn_{0.9}Fe_{0.1}O$−C, and $Sn_{0.9}Fe_{0.1}O_2$−C, respectively. These values are in rather good agreement with the experimentally determined ones (see Figure 4a), being just slightly (ca. 3%) higher (considering also the transition to (quasi-)amorphous phases, which has not been taken into account for the calculation). Accordingly, the relative porosity for a given volume decreases, while the total pore volume remains fairly constant.

To further investigate this, we performed a comparative *operando* dilatometry analysis of nonpressed and pressed (1t for one minute) $Zn_{0.9}Fe_{0.1}O$−C electrodes with the same mass loading. As a result of the pressing, the thickness of the coating layer decreased from 18 to 12 μm and the (calculated) porosity decreased from 66% to 49%. The dilatation during the first cycle of both electrodes (normalized by the specific capacity for clarity reasons) is shown in Figure 4b. It is observed that the variation in thickness is very similar with respect to the absolute (in micrometers) increase upon the first lithiation and decrease during the subsequent delithiation. Accordingly, the initial porosity does not "adsorb" the volume changes occurring at the particle level, which is different from what is commonly assumed, at least not to a large extent. Considering the relative increase with respect to the initial electrode thickness, however, the volume variation is apparently more pronounced in the case of the pressed electrodes (Figure 4c). Accordingly, the initial porosity has more a "diluting" effect in consideration of relative values.

In summary, we comprehensively analyzed the volume variation of three conversion/alloying materials, $ZnFe_2O_4$−C, $Zn_{0.9}Fe_{0.1}O$−C, and $Sn_{0.9}Fe_{0.1}O_2$−C, with a varying relative contribution of the alloying and conversion reaction. On the

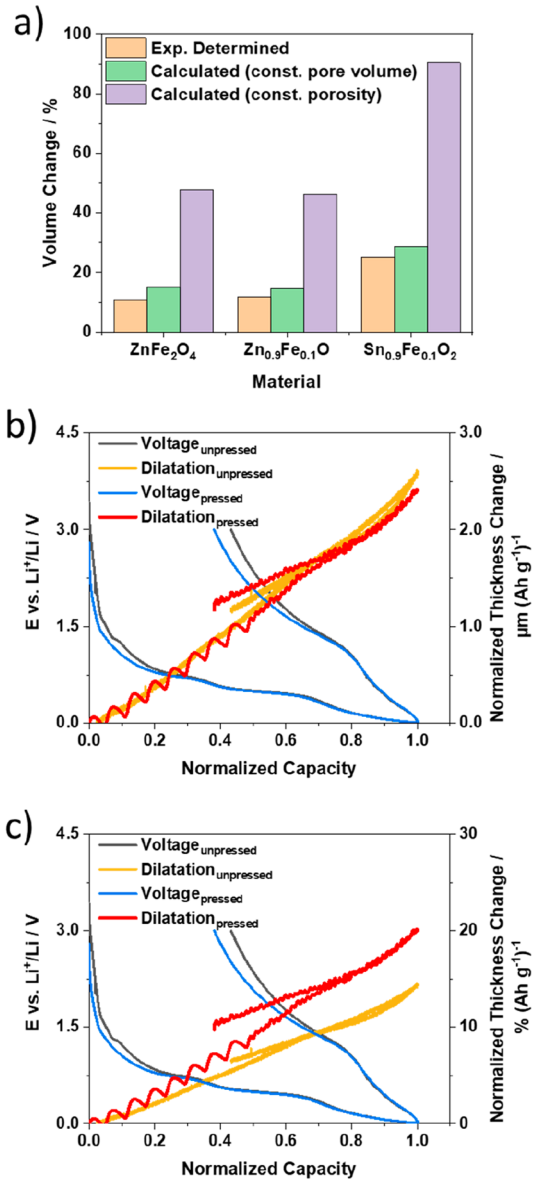

Figure 4. (a) Comparison of the experimentally determined reversible volume variation (in orange) for electrodes based on $ZnFe_2O_4$–C, $Zn_{0.9}Fe_{0.1}O$–C, and $Sn_{0.9}Fe_{0.1}O_2$–C with the reversible volume changes calculated for either a constant pore volume (in green) or a constant porosity (in purple). (b, c) Comparison of *operando* dilatometry data recorded for pressed and nonpressed electrodes based on $Zn_{0.9}Fe_{0.1}O$–C, including also the corresponding discharge/charge profiles. The capacity and thickness change have been normalized (the latter by the specific capacity) for clarity reasons. (b) depicts the normalized absolute volume changes in μm (Ah g ^{1}) ^{1}, and (c), the relative volume changes in % (Ah g ^{1}) ^{1}. Please note that the humps in the dilatation data of the pressed electrodes at lower potentials originate from some minor temperature fluctuation in the climatic chamber.

basis of the density of the initial and lithiated phases, a volume expansion of 113%, 120%, and 296% has been calculated at the particle level, revealing that an increasing ratio of the alloying reaction results in a more pronounced volume increase. This trend has been confirmed by *operando* dilatometry and backed-up exemplarily by *ex situ* cross-sectional SEM/FIB analysis. The overall reversible volume variation at the electrode level, however, is dramatically lower, i.e., only 10.7%, 11.8%, and 25.1% for $ZnFe_2O_4$–C, $Zn_{0.9}Fe_{0.1}O$–C, and $Sn_{0.9}Fe_{0.1}O_2$–C, respectively. While this is to a certain extent related to a buffering effect of the available void space inside the electrode, the total pore volume appears to remain fairly constant, according to our theoretical calculations. In fact, the comparison of pressed and nonpressed electrodes highlights that the initial porosity has more a "diluting" effect on the overall volume change rather than (largely) "adsorbing" the occurring volume change.

While these findings are generally providing some important insights into the relationship of theoretically expected and experimentally determined volume variations at the particle and electrode level and are anticipated to be applicable also to pure conversion and alloying materials, we may finally also note that all the volume changes reported herein refer to electrodes cycled within a very wide (though commonly employed) voltage window from 0.01 to 3.0 V, thus, essentially exploiting the maximum theoretical capacity. Limiting the applied anodic and cathodic cutoff voltages and, hence, the cycled capacity, will lead to substantially less pronounced reversible volume changes, which will be important for any potential commercial use of such high-capacity active materials.

AUTHOR INFORMATION

Corresponding Author

Dominic Bresser – *Helmholtz Institute Ulm (HIU), 89081 Ulm, Germany; Karlsruhe Institute of Technology (KIT), 76021 Karlsruhe, Germany;* orcid.org/0000-0001-6429-6048; Email: dominic.bresser@kit.edu

Authors

Jakob Asenbauer – *Helmholtz Institute Ulm (HIU), 89081 Ulm, Germany; Karlsruhe Institute of Technology (KIT), 76021 Karlsruhe, Germany*

Matthias Kuenzel – *Helmholtz Institute Ulm (HIU), 89081 Ulm, Germany; Karlsruhe Institute of Technology (KIT), 76021 Karlsruhe, Germany*

Tobias Eisenmann – *Helmholtz Institute Ulm (HIU), 89081 Ulm, Germany; Karlsruhe Institute of Technology (KIT), 76021 Karlsruhe, Germany*

Adele Birrozzi – *Helmholtz Institute Ulm (HIU), 89081 Ulm, Germany; Karlsruhe Institute of Technology (KIT), 76021 Karlsruhe, Germany*

Jeng-Kuei Chang – *Department of Materials Science and Engineering, National Chiao Tung University, Hsinchu 30010, Taiwan;* orcid.org/0000-0002-8359-5817

Stefano Passerini – *Helmholtz Institute Ulm (HIU), 89081 Ulm, Germany; Karlsruhe Institute of Technology (KIT), 76021 Karlsruhe, Germany;* orcid.org/0000-0002-6606-5304

Notes

The authors declare no competing financial interest.

ACKNOWLEDGMENTS

The authors thank the Vector Foundation within the NEW E^2 project, the KIT Young Investigator Network (YIN), as well as the Helmholtz Association for financial support.

REFERENCES

(1) Bresser, D.; Hosoi, K.; Howell, D.; Li, H.; Zeisel, H.; Amine, K.; Passerini, S. Perspectives of Automotive Battery R&D in China, Germany, Japan, and the USA. *J. Power Sources* **2018**, *382* (February), 176−178.

(2) Dunn, B.; Kamath, H.; Tarascon, J. M. Electrical Energy Storage for the Grid: A Battery of Choices. *Science* **2011**, *334* (6058), 928−935.

(3) Armand, M.; Tarascon, J. M. Building Better Batteries. *Nature* **2008**, *451* (7179), 652−657.

(4) Jow, T. R.; Delp, S. A.; Allen, J. L.; Jones, J.-P.; Smart, M. C. Factors Limiting Li^+ Charge Transfer Kinetics in Li-Ion Batteries. *J. Electrochem. Soc.* **2018**, *165* (2), A361−A367.

(5) Yamada, Y.; Iriyama, Y.; Abe, T.; Ogumi, Z. Kinetics of Lithium Ion Transfer at the Interface between Graphite and Liquid Electrolytes: Effects of Solvent and Surface Film. *Langmuir* **2009**, *25* (21), 12766−12770.

(6) Asenbauer, J.; Eisenmann, T.; Kuenzel, M.; Kazzazi, A.; Chen, Z.; Bresser, D. The Success Story of Graphite as a Lithium-Ion Anode Material − Fundamentals, Remaining Challenges, and Recent Developments Including Silicon (Oxide) Composites. *Sustain. Energy Fuels* **2020**. DOI: 10.1039/D0SE00175A

(7) Marinaro, M.; Bresser, D.; Beyer, E.; Faguy, P.; Hosoi, K.; Li, H.; Sakovica, J.; Amine, K.; Wohlfahrt-Mehrens, M.; Passerini, S. Bringing Forward the Development of Battery Cells for Automotive Applications: Perspective of R&D Activities in China, Japan, the EU and the USA. *J. Power Sources* **2020**, *459*, 228073.

(8) Lu, Y.; Yu, L.; Lou, X. W. Nanostructured Conversion-Type Anode Materials for Advanced Lithium-Ion Batteries. *Chem.* **2018**, *4* (5), 972−996.

(9) Yu, S.-H.; Lee, S. H.; Lee, D. J.; Sung, Y.-E.; Hyeon, T. Conversion Reaction-Based Oxide Nanomaterials for Lithium Ion Battery Anodes. *Small* **2016**, *12* (16), 2146−2172.

(10) Fang, S.; Bresser, D.; Passerini, S. Transition Metal Oxide Anodes for Electrochemical Energy Storage in Lithium-and Sodium-Ion Batteries. *Adv. Energy Mater.* **2020**, *10* (1), 1902485.

(11) Liu, D.; Liu, Z. jiao; Li, X.; Xie, W.; Wang, Q.; Liu, Q.; Fu, Y.; He, D. Group IVA Element (Si, Ge, Sn)-Based Alloying/Dealloying Anodes as Negative Electrodes for Full-Cell Lithium-Ion Batteries. *Small* **2017**, *13* (45), 1702000.

(12) Obrovac, M. N.; Chevrier, V. L. Alloy Negative Electrodes for Li-Ion Batteries. *Chem. Rev.* **2014**, *114*, 11444−11502.

(13) Jiang, Y.; Zhang, D.; Li, Y.; Yuan, T.; Bahlawane, N.; Liang, C.; Sun, W.; Lu, Y.; Yan, M. Amorphous Fe_2O_3 as a High-Capacity, High-Rate and Long-Life Anode Material for Lithium Ion Batteries. *Nano Energy* **2014**, *4*, 23−30.

(14) Jia, H.; Gao, P.; Yang, J.; Wang, J.; Nuli, Y.; Yang, Z. Novel Three-Dimensional Mesoporous Silicon for High Power Lithium-Ion Battery Anode Material. *Adv. Energy Mater.* **2011**, *1* (6), 1036−1039.

(15) Bresser, D.; Mueller, F.; Buchholz, D.; Paillard, E.; Passerini, S. Embedding Tin Nanoparticles in Micron-Sized Disordered Carbon for Lithium-and Sodium-Ion Anodes. *Electrochim. Acta* **2014**, *128*, 163−171.

(16) Cabana, J.; Monconduit, L.; Larcher, D.; Palacín, M. R. Beyond Intercalation-Based Li-Ion Batteries: The State of the Art and Challenges of Electrode Materials Reacting Through Conversion Reactions. *Adv. Mater.* **2010**, *22* (35), E170−E192.

(17) Bresser, D.; Passerini, S.; Scrosati, B. Leveraging Valuable Synergies by Combining Alloying and Conversion for Lithium-Ion Anodes. *Energy Environ. Sci.* **2016**, *9* (11), 3348−3367.

(18) Mueller, F.; Gutsche, A.; Nirschl, H.; Geiger, D.; Kaiser, U.; Bresser, D.; Passerini, S. Iron-Doped ZnO for Lithium-Ion Anodes: Impact of the Dopant Ratio and Carbon Coating Content. *J. Electrochem. Soc.* **2017**, *164* (1), A6123−A6130.

(19) Ma, Y.; Ma, Y.; Ulissi, U.; Ji, Y.; Streb, C.; Bresser, D.; Passerini, S. Influence of the Doping Ratio and the Carbon Coating Content on the Electrochemical Performance of Co-Doped SnO_2 for Lithium-Ion Anodes. *Electrochim. Acta* **2018**, *277*, 100−109.

(20) Ma, Y.; Ma, Y.; Giuli, G.; Diemant, T.; Behm, R. J.; Geiger, D.; Kaiser, U.; Ulissi, U.; Passerini, S.; Bresser, D. Conversion/Alloying Lithium-Ion Anodes − Enhancing the Energy Density by Transition Metal Doping. *Sustain. Energy Fuels* **2018**, *2* (12), 2601−2608.

(21) Birrozzi, A.; Asenbauer, J.; Ashton, T. E.; Groves, A. R.; Geiger, D.; Kaiser, U.; Darr, J. A.; Bresser, D. Tailoring the Charge/Discharge Potentials and Electrochemical Performance of SnO_2 Lithium-Ion Anodes by Transition Metal Co-Doping. *Batter. Supercaps* **2020**, *3* (3), 284−292.

(22) Mueller, F.; Bresser, D.; Chakravadhanula, V. S. K.; Passerini, S. Fe-Doped SnO_2 Nanoparticles as New High Capacity Anode Material for Secondary Lithium-Ion Batteries. *J. Power Sources* **2015**, *299*, 398−402.

(23) Bresser, D.; Mueller, F.; Fiedler, M.; Krueger, S.; Kloepsch, R.; Baither, D.; Winter, M.; Paillard, E.; Passerini, S. Transition-Metal-Doped Zinc Oxide Nanoparticles as a New Lithium-Ion Anode Material. *Chem. Mater.* **2013**, *25* (24), 4977−4985.

(24) Asenbauer, J.; Binder, J. R.; Mueller, F.; Künzel, M.; Geiger, D.; Kaiser, U.; Passerini, S.; Bresser, D. Scalable Synthesis of Micro-Sized Nanocrystalline $Zn_{0.9}Fe_{0.1}O$-C Secondary Particles and Their Use in $Zn_{0.9}Fe_{0.1}O$-C/$LiNi_{0.5}Mn_{1.5}O_4$ Lithium-Ion Full-Cells. *ChemSusChem* **2020**, *13*, 3504.

(25) Asenbauer, J.; Varzi, A.; Passerini, S.; Bresser, D. Revisiting the Energy Efficiency and (Potential) Full-Cell Performance of Lithium-Ion Batteries Employing Conversion/Alloying-Type Negative Electrodes. *J. Power Sources* **2020**, *473*, 228583.

(26) Liang, C.; Gao, M.; Pan, H.; Liu, Y.; Yan, M. Lithium Alloys and Metal Oxides as High-Capacity Anode Materials for Lithium-Ion Batteries. *J. Alloys Compd.* **2013**, *575*, 246−256.

(27) Choi, J. W.; Aurbach, D. Promise and Reality of Post-Lithium-Ion Batteries with High Energy Densities. *Nat. Rev. Mater.* **2016**, *1* (4), 1−16013.

(28) Noh, M.; Kwon, Y.; Lee, H.; Cho, J.; Kim, Y.; Kim, M. G. Amorphous Carbon-Coated Tin Anode Material for Lithium Secondary Battery. *Chem. Mater.* **2005**, *17* (8), 1926−1929.

(29) Kim, H.-K.; Roh, K. C.; Kim, K.-B. In Situ Electrochemical Dilatometric Study of Fe_3O_4/Reduced Graphene Oxide Nanocomposites as Anode Material for Lithium Ion Batteries. *J. Electrochem. Soc.* **2015**, *162* (12), A2308−A2312.

(30) Liu, X. H.; Zhong, L.; Huang, S.; Mao, S. X.; Zhu, T.; Huang, J. Y. Size-Dependent Fracture of Silicon Nanoparticles during Lithiation. *ACS Nano* **2012**, *6* (2), 1522−1531.

(31) Andre, D.; Hain, H.; Lamp, P.; Maglia, F.; Stiaszny, B. Future High-Energy Density Anode Materials from an Automotive Application Perspective. *J. Mater. Chem. A* **2017**, *5* (33), 17174−17198.

(32) Otero, M.; Heim, C.; Leiva, E. P. M.; Wagner, N.; Friedrich, A. Design-Considerations Regarding Silicon/Graphite and Tin/Graphite Composite Electrodes for Lithium-Ion Batteries. *Sci. Rep.* **2018**, *8* (1), 1−15851.

(33) Du, Z.; Dunlap, R. A.; Obrovac, M. N. High Energy Density Calendered Si Alloy/Graphite Anodes. *J. Electrochem. Soc.* **2014**, *161* (10), A1698.

(34) Pietsch, P.; Westhoff, D.; Feinauer, J.; Eller, J.; Marone, F.; Stampanoni, M.; Schmidt, V.; Wood, V. Quantifying Microstructural Dynamics and Electrochemical Activity of Graphite and Silicon-Graphite Lithium Ion Battery Anodes. *Nat. Commun.* **2016**, *7* (1), 1−12909.

(35) Karkar, Z.; Jaouhari, T.; Tranchot, A.; Mazouzi, D.; Guyomard, D.; Lestriez, B.; Roué, L. How Silicon Electrodes Can Be Calendered

without Altering Their Mechanical Strength and Cycle Life. *J. Power Sources* **2017**, *371*, 136−147.
(36) Vanpeene, V.; Villanova, J.; King, A.; Lestriez, B.; Maire, E.; Roué, L. Dynamics of the Morphological Degradation of Si-Based Anodes for Li-Ion Batteries Characterized by In Situ Synchrotron X-Ray Tomography. *Adv. Energy Mater.* **2019**, *9* (18), 1803947.
(37) Rezvani, S. J.; Mijiti, Y.; Gunnella, R.; Nobili, F.; Trapananti, A.; Minicucci, M.; Ciambezi, M.; Bresser, D.; Nannarone, S.; Passerini, S. Structure Rearrangements Induced by Lithium Insertion in Metal Alloying Oxide Mixed Spinel Structure Studied by X-Ray Absorption near-Edge Spectroscopy. *J. Phys. Chem. Solids* **2020**, *136*, 109172.
(38) Bresser, D.; Paillard, E.; Kloepsch, R.; Krueger, S.; Fiedler, M.; Schmitz, R.; Baither, D.; Winter, M.; Passerini, S. Carbon Coated $ZnFe_2O_4$ Nanoparticles for Advanced Lithium-Ion Anodes. *Adv. Energy Mater.* **2013**, *3* (4), 513−523.
(39) Giuli, G.; Eisenmann, T.; Bresser, D.; Trapananti, A.; Asenbauer, J.; Mueller, F.; Passerini, S. Structural and Electrochemical Characterization of $Zn_{1-x}Fe_xO$ - Effect of Aliovalent Doping on the Li^+ Storage Mechanism. *Materials* **2018**, *11* (1), 49.
(40) Asenbauer, J.; Hoefling, A.; Indris, S.; Tübke, J.; Passerini, S.; Bresser, D. Mechanistic Insights into the Lithiation and Delithiation of Iron-Doped Zinc Oxide: The Nucleation Site Model. *ACS Appl. Mater. Interfaces* **2020**, *12* (7), 8206−8218.
(41) Bresser, D.; Paillard, E.; Kloepsch, R.; Krueger, S.; Fiedler, M.; Schmitz, R.; Baither, D.; Winter, M.; Passerini, S. Carbon Coated $ZnFe_2O_4$ Nanoparticles for Advanced Lithium-Ion Anodes. *Adv. Energy Mater.* **2013**, *3* (4), 513−523.
(42) Wang, J.; Wang, L.; Zhang, S.; Liang, S.; Liang, X.; Huang, H.; Zhou, W.; Guo, J. Facile Synthesis of Iron-Doped SnO_2/Reduced Graphene Oxide Composite as High-Performance Anode Material for Lithium-Ion Batteries. *J. Alloys Compd.* **2018**, *748*, 1013−1021.
(43) Beattie, S. D.; Larcher, D.; Morcrette, M.; Simon, B.; Tarascon, J.-M. Si Electrodes for Li-Ion Batteries - A New Way to Look at an Old Problem. *J. Electrochem. Soc.* **2008**, *155* (2), A158.
(44) Martinez-Julian, F.; Guerrero, A.; Haro, M.; Bisquert, J.; Bresser, D.; Paillard, E.; Passerini, S.; Garcia-Belmonte, G. Probing Lithiation Kinetics of Carbon-Coated $ZnFe_2O_4$ Nanoparticle Battery Anodes. *J. Phys. Chem. C* **2014**, *118* (12), 6069−6076.
(45) Mueller, F.; Bresser, D.; Paillard, E.; Winter, M.; Passerini, S. Influence of the Carbonaceous Conductive Network on the Electrochemical Performance of $ZnFe_2O_4$ Nanoparticles. *J. Power Sources* **2013**, *236*, 87−94.
(46) Di Cicco, A.; Giglia, A.; Gunnella, R.; Koch, S. L.; Mueller, F.; Nobili, F.; Pasqualini, M.; Passerini, S.; Tossici, R.; Witkowska, A. SEI Growth and Depth Profiling on ZFO Electrodes by Soft X-Ray Absorption Spectroscopy. *Adv. Energy Mater.* **2015**, *5* (18), 1500642.
(47) Lin, K.-H.; Sun, S.-J.; Ju, S.-P.; Tsai, J.-Y.; Chen, H.-T.; Hsieh, J.-Y. Observation of the Amorphous Zinc Oxide Recrystalline Process by Molecular Dynamics Simulation. *J. Appl. Phys.* **2013**, *113* (7), 073512.
(48) Reddy, M. V.; Linh, T. T.; Hien, D. T.; Chowdari, B. V. R. SnO_2 Based Materials and Their Energy Storage Studies. *ACS Sustainable Chem. Eng.* **2016**, *4* (12), 6268−6276.
(49) Lee, J. H.; Lee, H. M.; Ahn, S. Battery Dimensional Changes Occurring during Charge/Discharge Cycles - Thin Rectangular Lithium Ion and Polymer Cells. *J. Power Sources* **2003**, *119*−*121*, 833−837.
(50) Aravindan, V.; Lee, Y.; Madhavi, S. Best Practices for Mitigating Irreversible Capacity Loss of Negative Electrodes in Li-Ion Batteries. *Adv. Energy Mater.* **2017**, *7* (17), 1602607.
(51) Holtstiege, F.; Bärmann, P.; Nölle, R.; Winter, M.; Placke, T. Pre-Lithiation Strategies for Rechargeable Energy Storage Technologies: Concepts, Promises and Challenges. *Batteries* **2018**, *4* (1), 4.
(52) Garrick, T. R.; Kanneganti, K.; Huang, X.; Weidner, J. W. Modeling Volume Change Due to Intercalation into Porous Electrodes. *J. Electrochem. Soc.* **2014**, *161* (8), E3297−E3301.
(53) Espinal, L. Porosity and Its Measurement. *Characterization of Materials*; John Wiley & Sons, Inc.: Hoboken, NJ, USA, 2012; pp 1−10.